Modeling Microwave-Enhanced Chemical Vapor Infiltration Process for Preventing Premature Pore Closure

Wenjun Ge*
Computational Sci. & Eng. Div.
Oak Ridge National Laboratory
Oak Ridge, TN 37831

Vimal Ramanuj
Computational Sci. & Eng. Div.
Oak Ridge National Laboratory
Oak Ridge, TN 37831

Mengnan Li
Computational Sci. & Eng. Div.
Oak Ridge National Laboratory
Oak Ridge, TN 37831

Ramanan Sankaran
Computational Sci. & Eng. Div.
Oak Ridge National Laboratory
Oak Ridge, TN 37831

Ying She
Physical Sciences Department
RTX Technologies Res. Center
East Hartford, CT 06108

Zissis Dardas
Physical Sciences Department
RTX Technologies Res. Center
East Hartford, CT 06108

ABSTRACT

The chemical vapor infiltration (CVI) process involves infiltrating a porous preform with reacting gases that undergo chemical transformation at high temperatures to deposit the ceramic phase within the pores, ultimately leading to a dense composite. The conventional CVI process in composite manufacturing needs to follow an isothermal approach to minimize temperature differences between the external and internal surfaces of the preform, ensuring that reactive gases infiltrate internal pores before external surfaces seal. This study addresses the challenge of premature pore closure in CVI processes through microwave heating. A frequency-domain microwave solver is developed in OpenFOAM to investigate volumetric heating mechanisms within the preform. Through numerical studies, we demonstrate the capability of microwave heating of creating an inside-out temperature inversion. This inversion accelerates reactions proximal to the preform center, effectively mitigating the risk of premature external pore closure and ensuring uniform densification. The results reveal a significant enhancement in temperature inversion when high-permittivity reflectors are incorporated to generate resonant waves. This microwave heating strategy is then coupled with high-fidelity direct numerical simulation (DNS) of reacting flow, enabling the analysis of resulting densification processes. The DNS includes detailed chemistry and realistic diffusion coefficients. The numerical results can be used to estimate the impact of microwave-induced temperature inversion on densification in productions.

Nomenclature

A Pre-exponential coefficient

*Corresponding author. Email: gew1@ornl.gov

This paper was presented at the ASME 2024 Summer Heat Transfer Conference (SHTC24) and has been revised from the version published in the conference proceedings [1].

C Progress variable
C_p Heat capacity
D Effective gas diffusivity
$\mathbf{E}$ Electric field
E_a Activation energy
f_E Microwave source term at the boundary
h Heat convection coefficient
I Surface microwave intensity
k Wave number
k_b Wave number at the boundary
L Material thickness
L_p Penetration depth
Q_{mw} Microwave heat source
S_I Deposition front speed
T Temperature
T_∞ Ambient temperature
ε Permittivity
κ Thermal conductivity
λ_c Characteristic wavelength
μ Permeability
ρ Material density
ρ_{gas} Gas density
ρ_s Deposited pase density
ϕ Porosity
ψ Level set function
ω Angular frequency
$\dot{\omega}_s$ Deposition rate
$\tan\delta$ Loss tangent

1 Introduction

Chemical vapor infiltration (CVI) is a technology used to produce ceramic matrix composites (CMC). The CMC synthesized through CVI exhibit exceptional mechanical properties under high temperature [2, 3]. In the CVI process, reactive gases diffuse and react with a porous preform (either fibers, or powders) until nearly full densification is achieved [4]. The quality of the resulting CMC is largely dependent on the final residual porosity, a parameter that remains challenging to control.

The conventional CVI operates as an isothermal-isobaric process. Both the gas precursor (e.g. CH_3SiCl_3 (MTS)/H_2 for SiC infiltration) and the preform are heated and maintained at the reaction temperature (900-1100 °C) under reduced pressure (1-10 kPa). Increasing the temperature and pressure would accelerate the deposition by theory, and therefore reduce the overall processing time. However, the infiltration of the reactants might be blocked due to the faster deposition rate close to the surface, the so-called, premature pore closure effect. The premature pore closure leads to residual porosity near the center of the preform, significantly degrading the synthesis quality of the CMC preform.

To avoid the premature pore closure, the temperature and pressure need to stay relatively low to slow down the reaction near the surface, facilitating the diffusion of the reactants into the center of the preform. Consequently, the conventional CVI becomes inherently time consuming, with the processing times typically ranging from 600 to 2000 hours.

Fundamentally, the premature closure problem in conventional CVI arises due to gas concentration gradient, with the concentration decreasing from the surface towards the preform center. In an isothermal process, the concentration gradient leads to a faster deposition rate near the surface compared to the internal regions. To address this challenge, researchers have explored various strategies to invert the density and/or temperature gradients [5–7]. These approaches aim to elevate the core temperature and/or reactants concentration above that of the external regions. Researchers at Oak Ridge National Laboratory [8, 9] invented a forced-flow/thermal-gradient method (FCVI), and were able to synthesize SiC-matrix components at a significantly higher temperature within a much shorter time frame. This is accomplished by heating from one side while infiltrating the gases from the opposite side.

Another promising approach to circumvent the premature closure involves the utilization of microwave heating [10–15]. Unlike conventional methods, microwave is able to heat a structure volumetrically, enabling heating up the preform inside-out during the CVI process. Devlin et al. [11] conducted experiments investigating the deposition of Si_3N_4 through microwave-assisted CVI. This study demonstrated inside-out densification under specific conditions, attributing to the inversion of temperature gradient generated by interactions between microwave and the material. Skamser et al. [12] adopted a hybrid

approach to heat the alumina preform with both microwave and thermal radiation. A susceptor is employed to increase the temperature around the preform to minimize the thermal runaway phenomenon. Jaglin et al. [13] investigated the microwave-assisted CVI for the production of SiC_f/SiC composites through X-ray absorptiometry and scanning electron microscopy. The experiments revealed inside-out densification with the center of the preform densified to 73% compared to the average density of 55% after 24 hours. They also observed that the initial inverse temperature profile obtained gradually flattened out after the densification front moved toward the edges. Binner et al. [14] improved microwave-assisted CVI to form SiC_f/SiC composites from SiC_f preforms by preimpregnating SiC powder. The samples loaded with powder showed higher infiltration rates, and average densities as high as 75% after 10 hours were achieved. In a pilot-scale initiative in Europe, D'Ambrosio et al. [15] outlined the design of a microwave-assisted CVI plant. The reactors in this pilot plant have the capacity to scale up the size of SiC preforms to twice that of lab-scale ones. The initial trials reached an average reaction efficiency (defined as the number of SiC moles deposited per MTS mole) of 25% with the desired inside-out densification enabled by microwaves.

While the application of microwave heating has demonstrated success in various laboratories and has been adopted in the industry, its utilization for heating and densifying porous ceramic structures presents unique challenges. The microwave-assisted CVI process is complex, involving coupled chemistry and physics at multiple scales. The underlying heating mechanism leading to the observed temperature gradient inversion remains unclear. When an incident microwave interferes with its reflection, the wave-shape heating pattern would be fundamentally different from those in conventional heating methods [16]. The temperature profile generated by the microwave changes over time due to the evolving preform porosity during densification [13, 17]. In addition, the uniformity of deposition depends on the competing effects of chemical kinetics and reactants diffusion, which the reaction rate has nonlinear dependency on the temperature through the modified Arrhenius relationship. All these pose difficulties in understanding the real cause and effect in the CVI process. More theoretical and computational insights are needed to interpret the experimental observations. There are very limited theoretical or computational studies [17–25] on this specific topic. An early pore-resolved simulation of microwave-enhanced CVI by Morell et al. [20], building on the initial models presented in [18, 19], demonstrated how the pattern of microwave power dissipation is influenced by both preform thickness and microwave frequency. Skamser et al. [22] developed a finite difference model for microwave-enhanced CVI, resolving the change of the composition by assuming a generalized equation for absorbed microwave power. This CVI model was also utilized to identify optimal conditions for producing dense ceramic matrix composites [23]. Tilley and Kriegsmann [24] introduced a 1-D sharp-interface model and outlined a heating strategy based on their simulation results. Goyal et al. [25] developed a multiphase model for microwave heating by using the microwave solver in COMSOL. Porter et al. [17] used a finite-difference time-domain solver implemented in QuickWave to explain the experimental observations, and found that when the SiC samples are small, the resulting energy coupling is very sensitive to the microwave frequency. They identified the important role of frequency in the microwave-assisted CVI process. Limited physics understanding and computational exploration pose a gap in this knowledge, which becomes the main motivation of this study. To facilitate wider adoption and scale-up of the technology, it is imperative to gain a fundamental understanding of the creation and the effects of the temperature inversion and quantified characterization of the process, especially regarding the relationships between the microwave frequency, size of the sample, characteristic wavelength, and the resonant waves within the preform.

In this study, a frequency-domain microwave solver is developed in OpenFOAM to investigate the microwave heating mechanism. The accuracy of the implementation is verified by comparing the results with established microwave heating examples in food processing. Subsequently, we apply the microwave solver to examine the conditions to generate the temperature inversion through standing waves. Through numerical simulations of microwave heating of β-SiC, we identify the necessary conditions to generate the resonant waves to obtain the inside-out temperature gradient inversions for different preform porosities. Finally, we applied the obtained temperature inversion to high-fidelity direct numerical simulation (DNS) of the reacting flow to model the process of infiltration and deposition.

2 Formulation

2.1 Governing equations

The governing equation for the electric field in the frequency domain in a source-free and isotropic medium is given by:

$$\nabla^2\mathbf{E} + k^2\mathbf{E} = 0\,, \tag{1}$$

$$k = \omega\sqrt{\mu\varepsilon}\,, \tag{2}$$

where $\mathbf{E}$ represents the electric field in phasor notation; k is known as the complex wave number; ω is the angular frequency; ε is the permittivity; μ is the permeability, which can be safely approximated by the permeability in the free space μ_0 for non-ferromagnetic materials in this study. The impedance boundary is used for the microwave solver for this study, which is

expressed as

$$\nabla_n E_n + jk_b E_n = f_E \ , \tag{3}$$

where E_n is the electric field component normal to the boundary; k_b is the wave number of the boundary; and f_E denotes any source introduced at the boundary. For a plane wave with an amplitude of E_0 perpendicular to the ceramic preform surface, f_E is defined by:

$$f_E = j(k_b + k)E_0 \ , \tag{4}$$

where E_0 is related to the wave intensity I_0 by

$$I_0 = \frac{1}{2}\left|\sqrt{\frac{\varepsilon}{\mu}}\right| E_0^2 \ . \tag{5}$$

In cases where no source is imposed at the boundary, $f_E = 0$.

The most critical property that characterize the microwave heating is the permittivity. Permittivity is a measure of the ease of electrical polarization in response to an external electric field. The permittivity is usually expressed in complex form, as given by

$$\varepsilon = \varepsilon' - \varepsilon'' j \ , \tag{6}$$

where ε' represents the real part, and ε'' represents the imaginary part. A useful parameter, so called the loss tangent or the dissipation factor, $\tan\delta$, is sometimes used for characterizing the heat loss in a dielectric material, which is defined as

$$\tan\delta = \frac{\varepsilon''}{\varepsilon'} . \tag{7}$$

The electromagnetic wave propagates in a material with a characteristic wavelength, defined as

$$\lambda_c = \frac{2\pi}{\mathfrak{Re}(k)} \ . \tag{8}$$

In a semi-infinity medium, the intensity of the electromagnetic wave decreases to approximately $1/e$ of its original value after penetrating a distance equal to the penetration depth L_p into the material. The L_p is defined as:

$$L_p = -1/\mathfrak{Im}(k) \ . \tag{9}$$

When an electromagnetic wave is mostly absorbed by the medium before being reflected, i.e. the thickness of the material $L \gg L_p$, there will be no standing wave formed within the material. The material will be heated following exponential decay, also known as the Beer-Lambert's Law.

After solving Eq. (1) for the electric field $\mathbf{E}$, the heating rate, or the microwave heat source, within the dielectric medium can be obtained by

$$Q_{\text{mw}} = \frac{1}{2}\omega\varepsilon''|\mathbf{E}|^2 \ . \tag{10}$$

Magnetic losses are usually negligible for most non-ferromagnetic materials.

The heat transfer equation needs to be solved to obtain the resulting temperature distribution within the preform under microwave heating. The microwave heat source, Q_{mw}, is represented as a source term to the heat transfer equation as

$$\rho c_p \frac{\partial T}{\partial t} - \kappa\nabla^2 T = Q_{\text{mw}} \ . \tag{11}$$

The boundary is subject to convection heat transfer:

$$-\kappa \nabla_n T = h(T - T_\infty) \ , \tag{12}$$

where ρ, c_p, κ, h are the density, specific heat capacity, thermal conductivity, and convection coefficient, respectively. Thermal radiative transfer is crucial for overall heat transfer, particularly when the preform is at elevated temperatures while the reactor wall is at a significantly lower temperature. However, accurately modeling radiative transfer for the preform requires solving the Radiative Transfer Equation (RTE) [26], which is beyond the scope of this study. Therefore, the effect of thermal radiative cooling of the preform is briefly discussed but not thoroughly addressed in this research.

The pore-scale reactive transport model used in this work was described in detail in [27], and implemented in the Quilt library [28]. Initial distribution of particles in the preform is represented using a level set function, ψ, such that its zero-contour corresponds to the particle surface. A representative volume element that resolves the thickness of the preform and is periodic in the two lateral directions is shown in Fig. 1. In typical CVI processing, the chemical kinetics time scales are several orders of magnitude shorter compared to gas transport. Hence, gas transport is assumed to be governed by steady-state diffusion given in dimensionless form as

$$\nabla^2 C = 0 \ \text{ with } \ \frac{\partial \mathrm{C}}{\partial \mathrm{n}}|_{\psi=0} = \frac{\dot{\omega}_\mathrm{s}}{\rho_\mathrm{gas} \mathrm{D}} \ , \tag{13}$$

where C is a progress variable representing the average gas composition. The far field condition $C = 1$ corresponds to the pyrolyzed state of the gaseous precursors. $C = 0$ corresponds to a state where all gaseous precursors have been depleted due to heterogeneous kinetics leading to solid phase deposition. The rate of consumption of C on the deposition front is expressed in terms of the deposition rate $\dot{\omega}_s$, gas phase density, ρ_{gas} and the effective diffusivity, D. The rate at which the deposition front advances can be expressed in terms of the deposition rate and solid phase density, ρ_s as

$$S_I = \frac{\dot{\omega}_s}{\rho_s} \ . \tag{14}$$

A continuous extension of the interface speed yields S_I, which is used to solve the transport of level set function as

$$\frac{\partial \psi}{\partial t} + S_I |\nabla \psi| = 0 \ . \tag{15}$$

The chemical kinetics of the gas phase pyrolysis and surface depositions using MTS/H_2 mixture as precursor are based on [29–31] and discussed in detail in [32] to evaluate $\dot{\omega}_s$ as a function of local temperature and C given in Arrhenius form:

$$\dot{\omega}_s(T, C) = k_s(T) C = A e^{-E_a/RT} C \ , \tag{16}$$

characterized by the pre-exponential coefficient, A and the effective activation energy, E_a. For the present work, these parameters are adopted from [27].

The microwave heating model described is implemented in the software platform, OpenFOAM [33, 34]. OpenFOAM is an open-source finite-volume library package that provides user-friendly C++ top abstractions for partial differential equations (PDEs). The original complex governing equation for microwave, Eq. (1) is split into two separate PDEs to solve for the real and imaginary parts in a segregated manner. Each PDE is solved by the conjugated gradient (CG) method. The temperature profile calculated by OpenFOAM is fed to the level-set DNS solver Quilt for densification simulations. For the fully coupled simulations, Quilt needs to return the porosity back to the OpenFOAM microwave solver to update the permittivity of the preform. However, due to the time scale differences, we only present the one-way coupling results in this study.

The schematic of the simulation geometry is shown in Fig. 1. The computational domain is scaled down to represent the densification differences primarily in the thickness direction. Microwave heating is effectively simplified as a one-dimensional simulation. The densification is simulated in 3-D with shortened transverse directions and lateral periodic boundary conditions. In all simulations conducted for this study, microwave heating is applied only to one side of the domain.

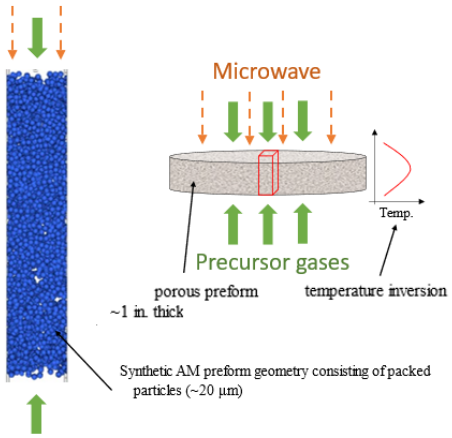

Fig. 1: Schematic of the simulation domain.

2.2 Dielectric and thermal properties of SiC

The permittivity of the porous material depends on the chemical composition of the material, frequency of the microwave, porosity, and temperature. This work focuses on β-SiC (3C-SiC) based ceramic packed-particle preforms being processed at the temperature range of 900-1250 °C (1173-1523 K) subject to a microwave with wavelength of 2.45 GHz. The bulk permittivity of β-SiC is from the experimental measurement of Sugawara et al. [35], while the thermal conductivity of β-SiC is from [36]. While both the permittivity ε and the thermal conductivity κ have temperature dependencies, we use the average values within the temperature range (1173-1523 K) instead of variable temperature-dependent properties. This could simplify the problem with the expectation that the temperature difference within the material is relatively small (< 150 K) during the CVI process. The temperature-averaged bulk properties used in this study is listed in Table 1.

Table 1: Permittivity and thermal conductivity of bulk β-SiC

Frequency of the microwave	f (GHz)	2.45
Real relative permittivity	$\varepsilon_s'/\varepsilon_0$	18.5
Imaginary relative permittivity	$\varepsilon_s''/\varepsilon_0$	8.8
Thermal conductivity	κ (W/m K)	13.7

The multi-phase properties are from the Maxwell-Garnett formula [37] for uniformly distributed spherical particles, which gives:

$$\varepsilon_{\text{eff}} = \varepsilon_g \frac{(\varepsilon_s + 2\varepsilon_g) + 2(1-\phi)(\varepsilon_s - \varepsilon_g)}{(\varepsilon_s + 2\varepsilon_g) - 2(1-\phi)(\varepsilon_s - \varepsilon_g)}, \tag{17}$$

where the subscript s denotes the solid phase, and the subscript g denotes the gas phase. The thermal conductivity follows the similar Maxwell-Garnett relationship to porosity ϕ [38]. The effective material properties for the porous β-SiC preform is calculated and listed in Table 2. The corresponding characteristic wavelength λ_c and penetration depth L_p are also calculated and listed in Table 2.

3 Results and discussion

3.1 Verification

Due to the lack of computational studies in microwave-assisted ceramic processing, the initial set of simulations are based on the applications of microwave heating in food processing. The food processing example is demonstrated previously by Ayappa et al. [39]. We simulate the same microwave heating example to verify the microwave heating solver, as well as to explain the physics insights of microwave heating.

Table 2: Effective material properties for porous β-SiC preform

ϕ	$\varepsilon'_{\text{eff}}/\varepsilon_0$	$\varepsilon''_{\text{eff}}/\varepsilon_0$	κ_{eff}, W/m K	λ_c, cm	L_p, cm
0.2	13.8	6.48	9.97	3.2	2.3
0.4	9.87	4.40	6.86	3.8	2.8
0.6	6.48	2.71	4.24	4.7	3.7
0.8	3.55	1.26	1.98	6.4	5.9

The food samples with specific thicknesses L are exposed to the incident microwave on one side. Both sides are subject to convection cooling by air in room temperature. The properties of the food samples and the microwave are listed in Table 3.

Table 3: Material properties and parameters for the food processing simulation

Frequency of the microwave	f (GHz)	2.45
Power density of the microwave	I (W/cm^2)	3
Real relative permittivity	$\varepsilon'/\varepsilon_0$	43
Imaginary relative permittivity	$\varepsilon''/\varepsilon_0$	15
Initial temperature	T_0 (K)	300
Thermal conductivity	κ (W/m K)	0.491
Density	ρ (kg/m^3)	1070
Heat capacity	c_p (J/kg K)	2850
Ambient temperature	T_∞ (K)	300
Heat convection coefficient	h (W/m^2 K)	2
Characteristic wavelength	λ_c (cm)	1.84
Penetration depth	L_p (cm)	1.73

The resulting microwave heat sources within the material and the transient evolution of temperature profiles are studied for samples with different sizes. Figure 2 shows the comparison of the simulation results with the reference [39] for three different sizes, with (a) for $L = \lambda_c/2$, (b) for $L = \lambda_c$, and (c) for $L = 2\lambda_c$. Both the predicted microwave heat source and temperature distributions from OpenFOAM numerical simulations match the reference solutions well. It can be seen that the sample size L, characteristic wavelength λ_c, and penetration depth L_p are critical parameters for microwave heat source patterns. When the size of the food sample is half of the characteristic wavelength λ_c, which is shown in Fig. 2(a), the heat source peaks at the edges of the food sample, and reaches its minimum close to the center of the sample. This is due to the resonance from the reflection at the food-air interfaces. The reflected wave travels in the opposite direction with the same wavelength and frequency as the incident wave, which forms a standing wave within the material. For this case shown in Fig. 2(a), the heat source generated by the standing wave exhibits its nodes at $\lambda_c/8$ and $3\lambda_c/8$, while its antinodes are at the center ($\lambda_c/4$) and the interfaces (0 and $\lambda_c/2$). This type of wave pattern cannot be predicted by the Beer-Lambert's law, which assumes a semi-infinite domain and results in the microwave heat source with the exponential decay profile from the entry. The penetration depth L_p, shown in Table 3, is very close to the characteristic wavelength λ_c. When the thickness of the sample is much larger than the penetration depth, more microwave energy is expected to get absorbed before reaching the other surface. Figure 2(c) shows the results for the sample size of $2\lambda_c$. The profile of the microwave heat source becomes more closely aligned with an exponential decay profile, diminishing the significance of the resonance effect.

Further, the corresponding temperature variations are also shown in Fig. 3 in space and time. Again, the temperature profile shows the expected exponential dependence on spatial location with its magnitude increasing in time for longer samples, while it shows the edge heating profile for the $L = 0.5\lambda_c$ sample. The temperature profiles generally follow the trend of the heat source profiles, while appearing much smoother. The temperature is subject to the heat transfer depending on the thermal conductivity within the material and convection at the interfaces.

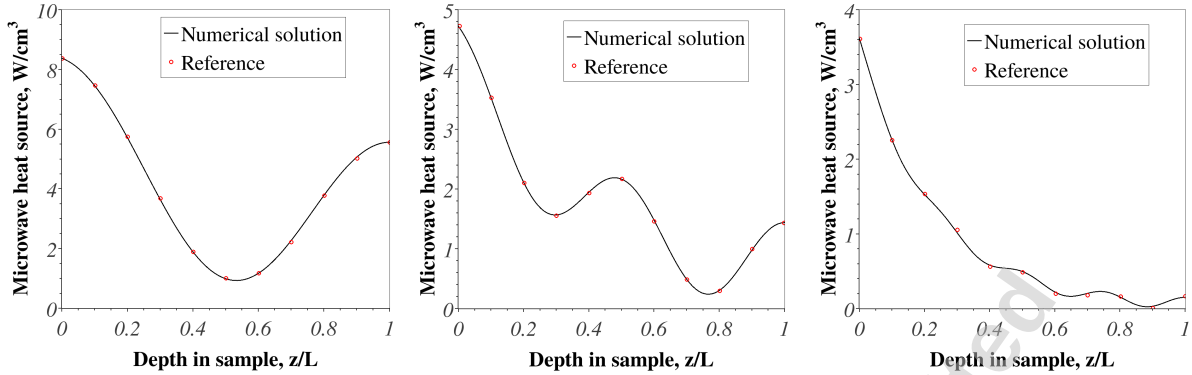

Fig. 2: Microwave heat source for the food samples with different lengths: (a) $L = 0.5\lambda_c = 0.92$ cm, (b) $L = \lambda_c = 1.84$ cm, and (c) $L = 2\lambda_c = 3.68$ cm.

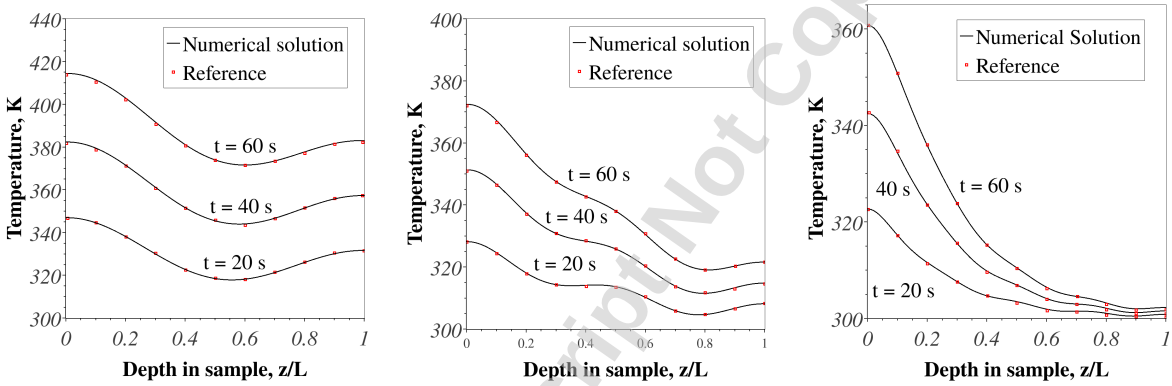

Fig. 3: Temperature distribution within the food samples at 20 s, 40 s, and 60 s with different sample lengths: (a) $L = 0.5\lambda_c = 0.92$ cm, (b) $L = \lambda_c = 1.84$ cm, and (c) $L = 2\lambda_c = 3.68$ cm.

3.2 Microwave-assisted CVI simulations

3.2.1 Temperature Inversion

In this Section, we utilize the verified microwave solver for β-SiC heating to identify the conditions for generating a temperature gradient inversion within the β-SiC preform. As was demonstrated in the previous example for food processing, the temperature distribution is governed by various geometric and microwave parameters. Key findings include

1. The preform thickness L should be smaller than $2L_p$ to generate a wave-like heating pattern. Otherwise, the microwave heating rate will be higher at the heating surface than the core.
2. Distinct standing wave patterns of a microwave heat source emerge when the sample size L is close to the characteristic wavelength λ_c of the microwave.
3. The peak of the standing wave should align with the center of the preform rather than any of the surfaces. This shift is essential to mitigate the 'edge heating' effect observed in the previous food processing example as shown in Fig. 2(a). Such 'edge heating' has also been reported by Jain et al. [40] for microwave-assisted thermal pasteurization. Here, 'edge heating' specifically refers to the peaks of the microwave heat source at the edges, rather than the peaks of the temperature distribution, which can be shifted inward through surface cooling.

Based on the these observations, we choose to simulate the microwave heating of β-SiC preform with the sample sizes of $L = 0.5\lambda_c$, where the λ_c for samples with different porosities are listed in Table 2. In actual production, while the sample size remains fixed, the microwave frequency can be adjusted to modulate the characteristic wavelength λ_c, ensuring it still meets the $L \approx 0.5L_c$ condition. Precise control of frequency within a certain range can be achieved through recent advancements in solid-state microwave systems [41,42].

Additionally, to enhance reflections and shift the standing wave peak towards the center, two thin porous layers with

relatively higher permittivity are introduced on each side. These reflector layers are porous, allowing gas transport, and possess high thermal conductivity to facilitate cooling at the outer surfaces. Figure 4 offers a schematic view of the enhanced microwave-assisted CVI process, showing the directions of precursor gases, preform and reflection layers, and the microwave heating direction and penetrations. The incident microwave is polarized and propagates normal to the surface.

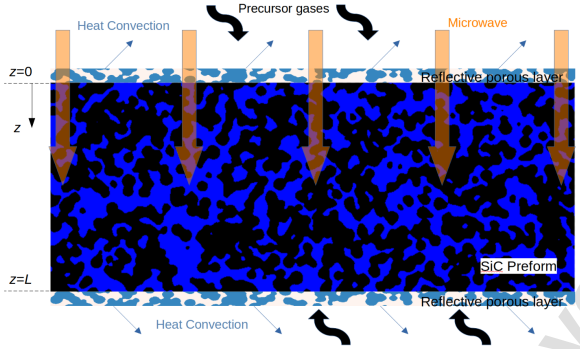

Fig. 4: Schematic of the enhanced microwave-assisted CVI process.

To show the differences, microwave heating of a porous β-SiC preform with and without the reflector layers are simulated and compared. The preform has a porosity (ϕ) of 0.2 and a thickness (L) of 1.6 cm. The incident microwave intensity at the upper surface ($z = 0$) is 3 W/cm^2 for both cases. In the scenario without the reflector, the SiC preform is directly exposed to the precursor gas, which has the same permittivity of air ($\varepsilon_{\text{air}} \approx \varepsilon_0$, and for this case $k_b = 51.4$). For the case with reflectors, the permittivity of the reflector material needs to be much higher than that of the SiC to shift the phase of the standing wave. The relative permittivity of the reflector used in this study is $420 - 71.4j$ (which gives a k_b of $1057 - 89j$). Several key constraints besides the high permittivity must be emphasized regarding the porous reflector to enable selection of material.

1. Thin: Since the idea is to only alter the dielectric property of the surfaces, the reflector needs to be as thin as possible to minimize the microwave absorption by the reflector.
2. Non-reactive: The material must be non-reactive with the gases so that the gaseous reagents can be transported to the preform without depletion. Moreover, depositions in the reflective layer could potentially close the pores and inhibit transport.
3. High porosity and large pores: The porous reflector should have higher porosity and pore sizes compared to the preform itself so that the infiltration does not encounter additional resistance.
4. The side of the reflector facing the incoming microwave needs to be less reflective (e.g. through anti-reflective coating). One can also position the reflector on just one side, allowing the microwave enters from the opposite side.
5. The radiative transfer effects are strongly dependent on the material and porosity of the reflector.

This study focuses on understanding the physics mechanism for generating the inside-out heating patterns by microwave within the preform. While the optimal choice of the reflector material and the above constraints in the real production requires further investigation, for the purpose of proof of concept, the same reflector material is employed consistently in the simulations throughout the paper. The results in terms of microwave heat source are shown in Fig. 5(a), and the desired microwave heating pattern is obtained with the peak of standing wave close to the center of the preform when the reflectors are added. Meanwhile, the microwave heat source without the reflector has the shape similar to the food processing case in Fig. 2(a) and SiC heating case in the literature [20] with the peaks at the edges.

Next, we study the heat transfer within the SiC preform, aiming for a reaction temperature range of 900-1100°C (1173–1373 K). Achieving the temperature inversion also requires forced convection, in addition to the inversion of the microwave heating rates. The gas flow speed in the reactor needs to be higher than in conventional reactors. An effective convection coefficient h_{eff} around 100 W/m^2 is used for the heat transfer simulations. In a previous simulation study [20], 330 W/m^2 is recommended as optimum for its condition examined. Since the reflector is thin and with high thermal conductivity, and $h_{\text{eff}} = 1/(1/h_{\text{inf}} + L_{\text{ref}}/\kappa_{\text{ref}})$, the effects of reflectors on the heat transfer can be safely ignored. The surrounding gas temperature T_{inf} should be lower, within the range of 200-600°C (473–873 K). In a conventional furnace, the gases will be at a higher temperature to allow for the pyrolysis reactions before reaching the preform. However, with the microwaves responsible for heating the preform, reagents might pyrolyze upon entering the preform rather than in the reactor chamber. This change has the potential to reduce the overall energy consumption of the entire CVI process, comparing to energy consumption required to maintain the entire reactor at an elevated temperature. The thermal conductivity κ of the preform also plays an crucial

role. At higher porosity (smaller κ), larger temperature gradients within the preform are expected, combined with the heat source inversion and the surface convection. As the preform becomes denser (larger κ), the temperature gradient should decrease, as was observed in the experiment [13]. In the production, change of microwave frequency and power is necessary to maintain the wanted temperature inversion.

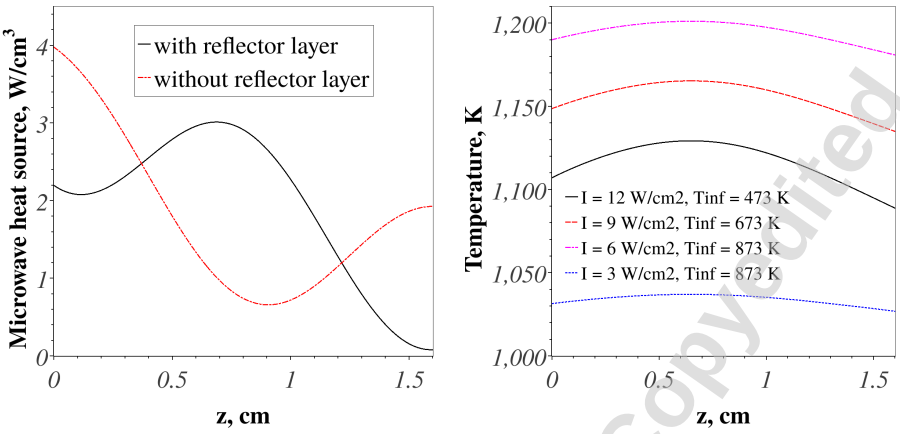

(a) (b)

Fig. 5: Distributions of (a) microwave heat source under the microwave power density of $I = 3$ W/cm^2 on one side ($z = 0$ cm), and (b) steady-state temperature for the SiC sample with porosity ϕ=0.2, $L = 0.5\lambda_c = 1.6$ cm, and the effective heat convection coefficient h_{eff} = 100 W/m^2 K.

The steady-state temperature profiles for the β-SiC with $\phi = 0.2$ are shown in Fig. 5(b) to show the temperature gradient inversions under different incident microwave power and ambient temperatures. Table 4 summarises the simulation results in terms of two quantities: the minimum temperature T_{min} at the non-heated surface ($z = L$), and the difference between the core and surface temperatures, $\Delta T = T_{\text{max}} - T_{\text{min}}$. The outcome has shown that microwave is able to generate the temperature inversions under these realistic reactor conditions with the help of reflectors. Different combinations of parameters yield different inverted temperature profiles. High microwave power (12 W/cm^2) with low ambient temperature (473 K) produces a substantial temperature inversion ($\Delta T = 40$ K), but the temperature range (1089–1129 K) might be too low for effective densification. Low microwave power (3 W/cm^2) with high ambient temperature (873K) results in a limited temperature inversion ($\Delta T = 10K$). The case with $I = 6$ W/cm^2, $T_\infty = 873$ K yields a suitable temperature profile for densification, with T_{min}=1181 K and $\Delta T = 20$K.

Table 4: Summary of the temperature inversion within the SiC preform ($\phi = 0.2$, $L = 1.6$ cm)

I, W/cm^2	E_0, V/m	T_∞, K	T_{min}, K	ΔT, K
3	2407	873	1027	10
6	3405	873	1181	20
9	4170	673	1135	30
12	4816	473	1089	40

Temperature gradient inversion can also be achieved at other porosities. The steady-state temperature distributions for β-SiC with $\phi = 0.6$ are studied next, with a preform thickness L of 2.35 cm. Two conditions are studied, including one case (HILT) with higher microwave power (9 W/cm^2) and lower ambient temperature (723 K), and the other (LIHT) with lower microwave power (6 W/cm^2) and higher ambient temperature (823 K). The microwave heat source and the resulting temperature profiles are shown in Fig. 6. Compared to the $\phi = 0.2$ preform, which has a higher thermal conductivity, the temperature inversions in the $\phi = 0.6$ preform show larger temperature difference between the surface and core, with the $\Delta T_{\text{LIHT}} = 75$ K and $\Delta T_{\text{HILT}} = 113$ K. The potential major benefit of microwave-assisted CVI is to increase the overall preform temperature without premature pore closure, allowing for a substantial reduction in processing time. Regarding this,

the HILT temperature profile seems to outperform the LIHT one for the densification. Densification simulations are required for further analysis, which will be conducted and analyzed in the next section.

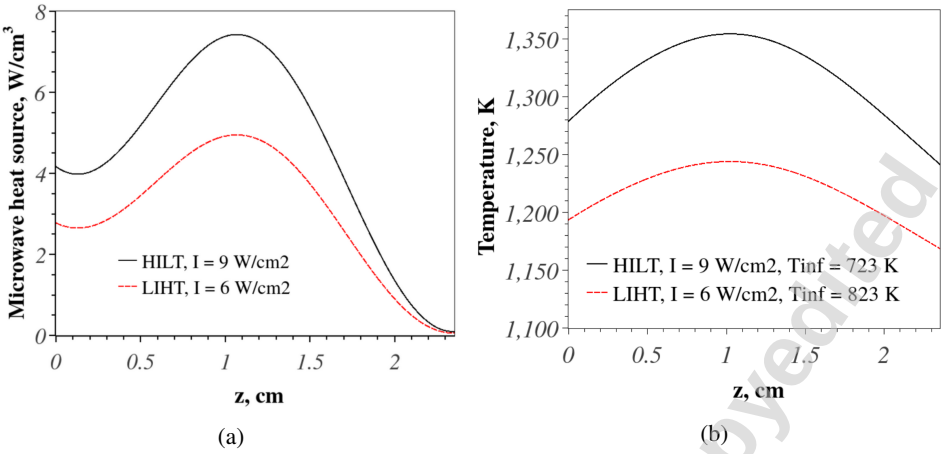

Fig. 6: Distributions of (a) microwave heat source under the microwave power density of $I = 6$ W/cm^2 and $I = 9$ W/cm^2 on one side ($z = 0$ cm), and (b) steady-state temperature for the SiC sample with porosity ϕ=0.6, $L = 0.5\lambda_c = 2.35$ cm, and the surface heat convection coefficient h_{eff} = 100 W/m^2 K.

The effect of radiative transfer is briefly discussed next, based on the HILT example. Radiative transfer influences overall heat transfer in two key aspects: first, through heat exchange between the outer preform surface and the reactor wall, and second, via radiative transfer within the porous preform. For the former, the preform loses extra heat through its surface in addition to the convection. To account for this, and considering the uncertainty regarding the radiative properties of the reflector, a linearized radiative transfer coefficient h_{rad}, ranging from 100 to 300 W/m^2, is added the effective heat transfer coefficient h_{eff}. For the later, hotter surfaces within the preform radiatively heat cooler surfaces inside the preform. This effect is approximately incorporated by increasing κ_{eff} by 10-30%. The results, as shown in Fig. 7, demonstrate the potential magnitude of radiative cooling effects comparing to the original HILT condition. While it is clear that detailed radiation evaluation is necessary for optimizing the CVI processing, due to the scope of this study, radiative transfer will not be considered in the densification simulation to allow for more controlled analysis.

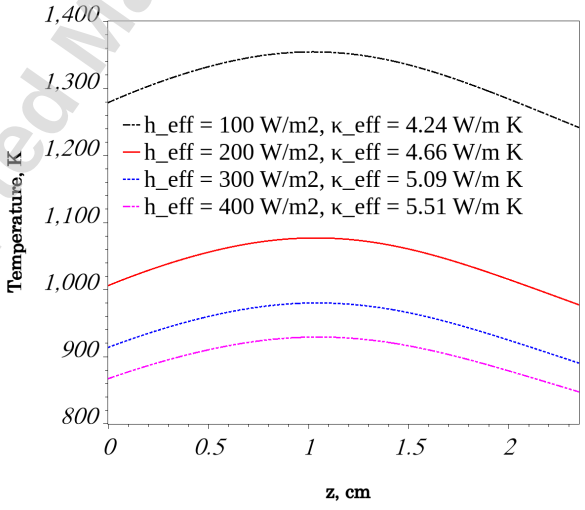

Fig. 7: Comparison of temperature profiles including simplified radiation effects for the SiC sample with porosity ϕ=0.6, $L = 0.5\lambda_c = 2.35$ cm, microwave intensity I = 9 W/m^2, and ambient temperature $T_{\text{inf}} = 723$ K.

3.2.2 Densification simulation

Densification is simulated to quantify the effects of temperature inversion on the synthesis quality of the preform. The densification behavior under different temperature distributions are analyzed: uniform and inverted temperature profiles using microwave heating. Firstly, a simplified 1-D form of Eq. (13) is solved assuming a uniform specific surface area distribution. Subsequently, the deposition rate is obtained from the distribution of C and the temperature profile. Figure 8 shows the deposition rate distribution for two uniform temperature cases. Following key observations can be made. Naturally, the high temperature case showed faster kinetics (depositions). The deposition rate near the outer surface for the 950° C (1223 K) is more than twice that of the 900° C (1173 K). Faster kinetics near the outer surface and slow in the core at high temperature leads to premature surface closure and leaves the core highly porous. Meanwhile, low temperature processing shows a more uniform deposition rate. However, a slow deposition rate means that the processing times are much longer.

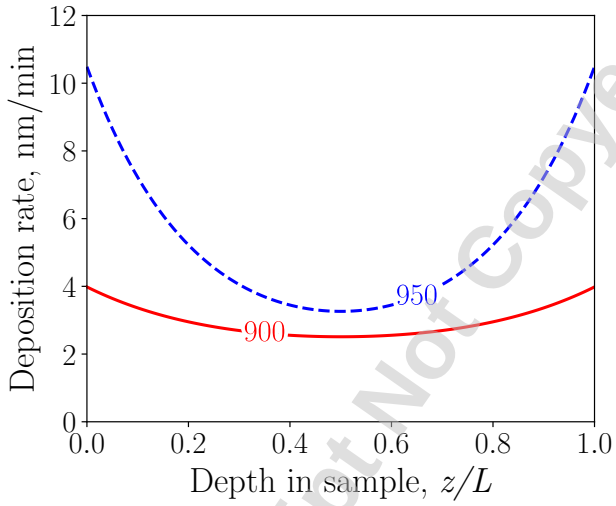

Fig. 8: Distribution of deposition rates for uniform temperature cases.

As previously described, inverted temperature distributions can potentially overcome the composition depletion in the core and lead to densification inside-out. However, the core temperature needs to be high enough to overcome this deficit. We study the deposition rates by varying the core temperature keeping the surface temperature constant (900°C or 1173 K). Figure 9 shows various cases with the core temperature being up to 50 K higher than the surface. It is observed that the core temperature must be higher than a certain threshold to cause an inversion in the deposition rate and ultimately obtain inside-out densification. Results from Figs. 8 and 9 demonstrate the motivation for controlling the temperature distribution within a porous preform in CVI to achieve inside-out densification that can avoid premature pore closures.

Following the above preliminary analyses, we study the deposition rates obtained from particle resolved 3-D densification simulations using the microwave heating temperature profiles as shown in Fig. 6(b) from the previous section. The resulting gas composition distribution and deposition rate along the thickness of the preform are shown in Fig. 10(a) and Fig. 10(b), respectively. Since Profile HILT has a higher surface temperature compared to Profile LIHT, the surface kinetics rate in HILT is higher which leads to faster depletion of the composition along the thickness. The deposition rate on the surface of the preform in case HILT is almost 4× that of case LIHT. On the contrary, deposition rate in the core shows the opposite behavior with the resulting deposition rate of LIHT higher than that of the HILT. Consequently, the core temperature in HILT is not high enough to compensate the low concentration as seen in Fig. 10(b). The LIHT temperature profile outperforms the HILT case for densification. The deposition rate is successfully inverted. This is a key observation in understanding the densification characteristics in microwave assisted CVI.

The instantaneous deposition rate shown in Fig. 10(b) seems promising. To quantitatively analyze the densification behavior through the entire CVI process, we performed pore-resolved 3-D DNS simulations of the CVI process using the microwave-heated temperature distributions, and compared them with a uniform isothermal processing case at 1000°C (1273 K). The simulation is conducted under the assumption that the preform is maintained at the same temperature inversion throughout the densification. A representative volume element (RVE) used in the simulations is shown in Fig. 11. The packed particles are initialized as randomly distributed spheres with the size distribution following [32]. Figures 11 (b) and (c) also show the mid-plane slices of the domain to clearly visualize the particles. The average density of the initial packing is approximately 0.22. Further, the study focuses on densification within the core and outer surface as outlined in the figure.

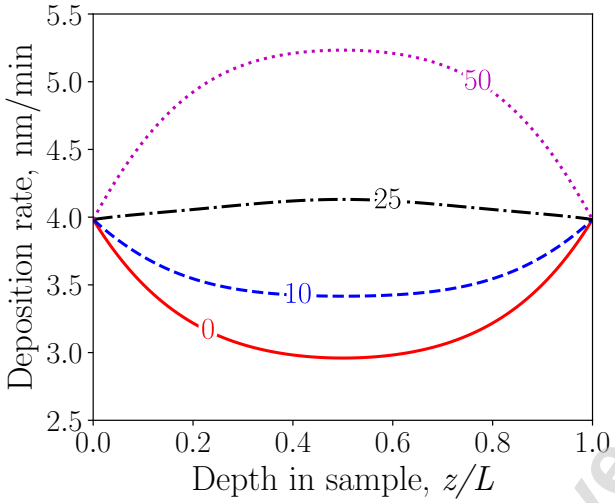

Fig. 9: Distribution of deposition rates for different inverted temperature profiles. The surface temperature is kept at 900°C (1173 K).

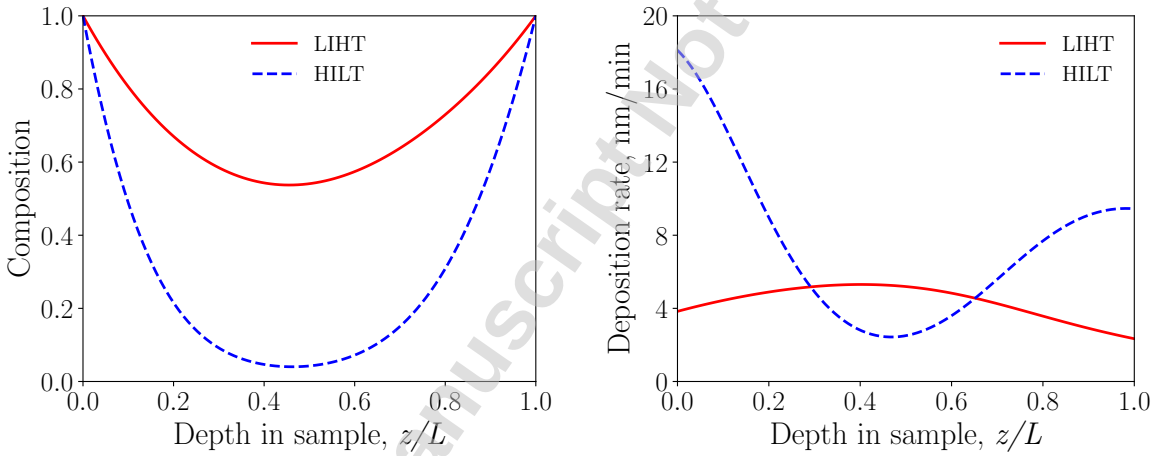

(a) (b)

Fig. 10: Composition (a) and deposition rate (b) distributions for the inverted temperature profiles using microwave heating.

Since the density distribution along the preform thickness is of importance, solid volume fraction within the domain is averaged along the periodic directions. The resulting density distribution is shown in Fig. 12. We observe that the density throughout the thickness direction is below 0.8 for the uniform temperature case (1000° C or 1273 K) with a noticeable gradient towards the outer surfaces. Note that the distribution also reflects characteristics of the initial non-uniform (random) porosity distribution within the preform. Next, we analyze the densification results using the microwave temperature profiles: LIHT and HILT. Corresponding to the trend observed in the deposition rate, core density in HILT is considerably lower than in LIHT. There is only marginal growth of the solid phase in HILT particularly within the core. Both cases show similar densities (85%) near the outer surface. However, density in the core for the HILT case is 50% while that in LIHT reaches 80%. It can be inferred that the density distribution for the LIHT profile is relatively much uniform and higher than the HILT case. This is consistent with the observation of [22], which discussed the benefit of smaller temperature gradients. These results clearly demonstrate the suitability of temperature inversion achieved using microwave heating for improving the densification quality of a porous preform.

The DNS simulations have shown that the densification quality depends on a delicate balance between chemical reaction, gas diffusion, and temperature inversion. The pathway to accelerating high-quality densification through microwave-generated temperature inversion has been demonstrated. Careful tuning of the CVI conditions is necessary to pinpoint the conditions to get an inside-out densification. Such optimization requires fully-coupled simulation and experimental charac-

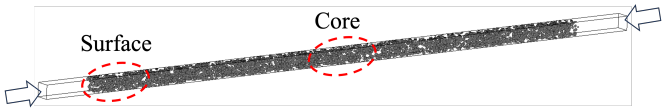

(a) Schematic

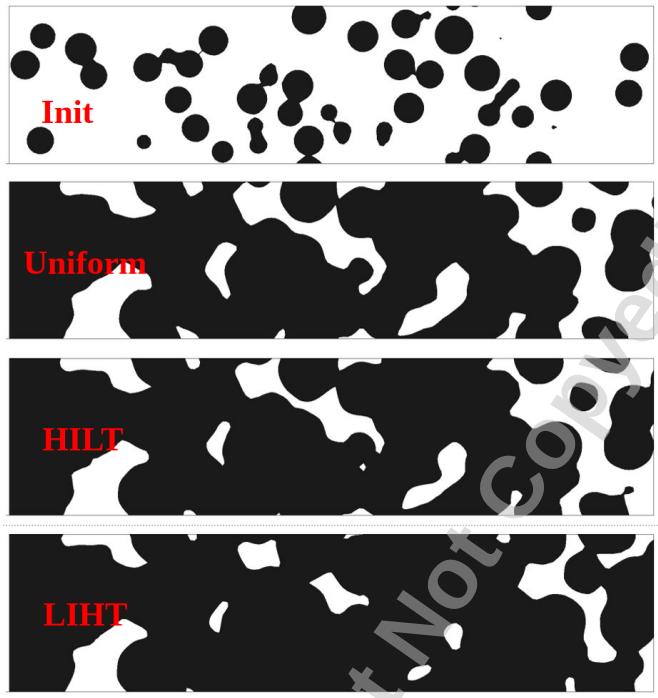

(b) Surface

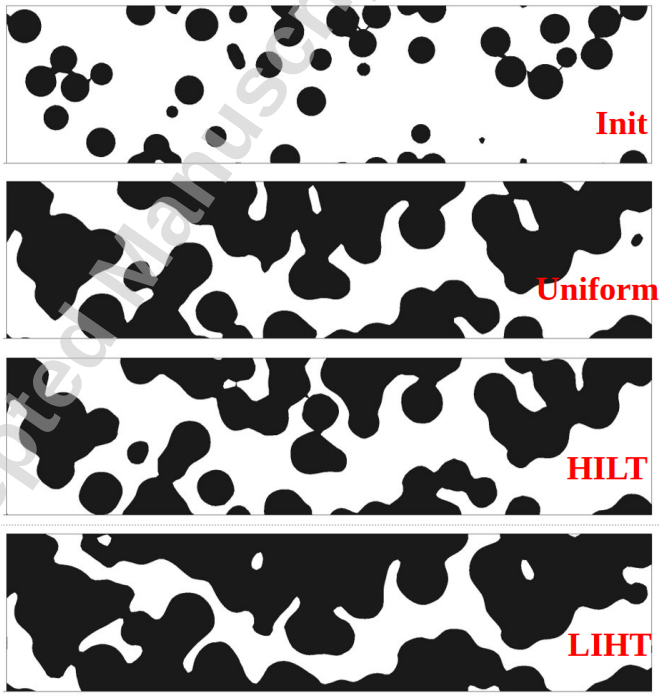

(c) Core

Fig. 11: Pore-resolved densification using uniform and inverted temperature profiles.

terizations.

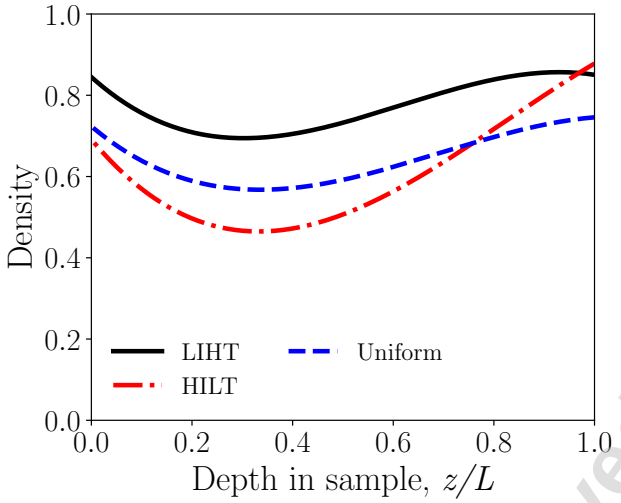

Fig. 12: Density distribution using uniform and inverted temperature profiles from the pore-resolved simulations.

4 Conclusions

This computational study focused on accelerating the CVI process by microwave heating. We had shown that the temperature gradient inversion created by the resonant microwave with the β-SiC preform can significantly reduce the risk of premature pore closure. The mechanism of microwave heating, and the necessary conditions to generate a standing wave that has its peak at the core of the preform were analyzed. We also coupled the microwave-heated temperature profile to the pore-resolved DNS simulations. The results have shown that even with the temperature inversion, premature pore closure can still happen due to faster reaction rate at the surfaces and limited precursor transport, especially at a later stage of the CVI densification. However, we had shown promising densification results which reduced the risk of premature disclosure significantly compared to the isothermal synthesis at a similar temperature level. The conclusions drawn from the simulations are:

1. The size and the permittivity of the material determine whether the heating pattern would be wave-like or following the exponential decay from the surface.
2. Reflection of the microwave at the material surface is critical to enable the inside-out heating pattern and shift the peak towards the core.
3. The microwave-assisted CVI process is a delicate combination of chemical reaction, precursor gas diffusion, and microwave heating.

In future studies, it is essential to address the limitations identified in this work. Further investigation into the materials and parameters of the reflector is necessary through both experiments and simulation approaches. A more comprehensive heat transfer model should include detailed simulation of radiative heat transfer. Incorporating temperature-dependent material properties will enhance the fidelity of the simulations and enable a better assessment of thermal runaway scenarios. Additionally, fully-coupled modeling at pore scale could provide more insights into optimizing the microwave-assisted chemical vapor infiltration process. These advancements will contribute to a deeper understanding of the underlying mechanisms and facilitate the development of more efficient industrial applications. Furthermore, additional strategies can be explored alongside microwave heat source inversion, including pulsed microwave [19], optimization of the initial ratio of the reactant mixture [23], and the use of multifrequency microwave sources [42].

Acknowledgements

This research was supported by the High-Performance Computing for Manufacturing Program (HPC4Mfg), managed by the U.S. Department of Energy (DOE), Advanced Manufacturing Office (AMO) within the Energy Efficiency and Renewable Energy (EERE) Office. This research used resources of the Oak Ridge Leadership Computing Facility (OLCF) and Compute and Data Environment for Science (CADES) at the ORNL, which is supported by the Office of Science of the U.S. DOE under Contract No. DE-AC05-00OR22725. The authors acknowledge the contributions of Jake Parsons and Christopher Ibarra whose internships were supported by HPC4Mfg Internship Program.

References

[1] Ge, W., Ramanuj, V., Li, M., Sankaran, R., She, Y., and Dardas, Z., 2024. "Modeling microwave-enhanced chemical vapor infiltration process for preventing premature pore closure". In Proc. ASME 2024 Heat Transf. Summer Conf. (SHTC24), p. V001T10A001.

[2] Kennedy, J. M., Moeller, H. M., and Johnson, W. S., 1990. *Thermal and mechanical behavior of metal matrix and ceramic matrix composites*, Vol. STP 1080. ASTM International.

[3] Campbell Jr, F. C., Campbell Jr, F. C., ed., 2011. *Manufacturing technology for aerospace structural materials*. Elsevier, ch. Ceramic matrix composites.

[4] Leuchs, M., Krenkel, W., ed., 2008. *Ceramic matrix composites: fiber reinforced ceramics and their applications*. J. Wiley & Sons, ch. Chemical vapor infiltration processes for ceramic matrix composites: manufacturing, properties, applications.

[5] Probst, K. J., Besmann, T. M., Stinton, D. P., Lowden, R. A., Anderson, T. J., and Starr, T. L., 1999. "Recent advances in forced-flow, thermal-gradient CVI for refractory composites". *Surf. Coat. Technol.,* **120**, pp. 250–258.

[6] Leonelli, C., and Veronesi, P., Bansal, N. P., and Boccaccini, A. R., eds., 2012. *Ceramics composites processing methods*. J. Wiley & Sons, ch. Microwave processing of ceramic and ceramic matrix composites.

[7] Vignoles, G. L., Descamps, C., Charles, C., and Klein, C., 2023. "How is it possible to get optimal infiltration fronts during chemical vapor infiltration with thermal gradients?". *Open Ceram.,* **15**, p. 100375.

[8] Moeller, H. H., Long, W. G., Caputo, A. J., and Lowden, R. A., 1986. "SiC fiber reinforced SiC composites using chemical vapor infiltration". *SAMPE Q.;(US),* **17**(3).

[9] Weaver, B. L., Lowden, R. A., McLaughlin, J. C., Stinton, D. P., Besmann, T. M., and Schwarz, O. J., 1993. "NextelTM/SiC composites fabricated using forced chemical vapor infiltration". In Proc. 17th Annu. Conf. Compos. Adv. Ceram. Mater., Wiley Online Library, pp. 1007–1015.

[10] Janney, M. A., Kimrey, H. D., and Kiggans, J. O., 1992. "Microwave processing of ceramics: Guidelines used at ORNL". *MRS Online Proc. Libr.,* **269**.

[11] Devlin, D. J., Currier, R. P., Barbero, R. S., and Espinoza, B. F., 1993. "Chemical vapor infiltration with microwave heating". *Ceram. Eng. Sci. Proc.,* **14**(9–10), pp. 761–767.

[12] Skamser, D. J., Day, P. S., Jennings, H. M., and Johnson, D. L., 1994. "Hybrid microwave-assisted chemical vapor infiltration of alumina fiber composites". In Proc. of the 18th Annu. Conf. on Compos. Adv. Ceram. Mater. B: Ceram. Eng. Sci. Proc., Wiley Online Library, pp. 916–923.

[13] Jaglin, D., Binner, J., Vaidhyanathan, B., Prentice, C., Shatwell, B., and Grant, D., 2006. "Microwave heated chemical vapor infiltration: densification mechanism of SiCf/SiC composites". *J. Am. Ceram. Soc.,* **89**(9), pp. 2710–2717.

[14] Binner, J., Vaidhyanathan, B., and Jaglin, D., 2013. "Microwave heated chemical vapour infiltration of SiC powder impregnated SiC fibre preforms". *Adv. Appl. Ceram.,* **112**(4), pp. 235–241.

[15] D'Ambrosio, R., Aliotta, L., Gigante, V., Coltelli, M., Annino, G., and Lazzeri, A., 2021. "Design of a pilot-scale microwave heated chemical vapor infiltration plant: An innovative approach". *J. Eur. Ceram. Soc.,* **41**(5), pp. 3019–3029.

[16] Sturm, G. S., Verweij, M. D., Van Gerven, T., Stankiewicz, A. I., and Stefanidis, G. D., 2012. "On the effect of resonant microwave fields on temperature distribution in time and space". *Int. J. Heat Mass Transf.,* **55**(13-14), pp. 3800–3811.

[17] Porter, M. T., Binner, J., Cinibulk, M. K., Stern, K. E., and Yakovlev, V. V., 2023. "Computational characterisation of microwave heating of fibre preforms for CVI of SiCf/SiC composites". *J. Eur. Ceram. Soc.,* **43**(5), pp. 1808–1827.

[18] Morell, J. I., Economou, D. J., and Amundson, N. R., 1992. "A mathematical model for chemical vapor infiltration with volume heating". *J. Electrochem. Soc.,* **139**(1), p. 328.

[19] Morell, J. I., Economou, D. J., and Amundson, N. R., 1992. "Pulsed-power volume-heating chemical vapor infiltration". *J. Mater. Res.,* **7**(9), pp. 2447–2457.

[20] Morell, J. I., Economou, D. J., and Amundson, N. R., 1993. "Chemical vapor infiltration of SiC with microwave heating". *J. Mater. Res.,* **8**(5), pp. 1057–1067.

[21] Gupta, D., and Evans, J. W., 1993. "Mathematical model for chemical vapor infiltration in a microwave-heated preform". *J. Am. Ceram. Soc.,* **76**(8), pp. 1924–1929.

[22] Skamser, D. J., Thomas, J. J., Jennings, H. M., and Johnson, D. L., 1995. "A model for microwave processing of compositionally changing ceramic systems". *J. Mater. Res.,* **10**(12), pp. 3160–3178.

[23] Skamser, D. J., Jennings, H. M., and Johnson, D. L., 1997. "Model of chemical vapor infiltration using temperature gradients". *J. Mater. Res.,* **12**(3), pp. 724–737.

[24] Tilley, B., and Kriegsmann, G., 2001. "Microwave-enhanced chemical vapor infiltration: a sharp interface model". *J. Eng. Math.,* **41**, pp. 33–54.

[25] Goyal, H., and Vlachos, D. G., 2020. "Multiscale modeling of microwave-heated multiphase systems". *Chem. Eng. J.,* **397**, p. 125262.

[26] Ge, W., David, C., Modest, M. F., Sankaran, R., and Roy, S. P., 2023. "Comparison of spherical harmonics method and discrete ordinates method for radiative transfer in a turbulent jet flame". *J. Quant. Spectrosc. Radiat. Transf.,* **296**,

p. 108459.

[27] Ramanuj, V., Li, M., Ge, W., Sankaran, R., She, Y., and Dardad, Z., 2024. "Effects of temperature inversion on densification in chemical vapor infiltration". *J. Am. Ceram. Soc.*, pp. 1–14.

[28] Ramanuj, V., and Sankaran, R., 2019. "High order anchoring and reinitialization of level set function for simulating interface motion". *J. Sci. Comput.,* **81**(3), pp. 1963–1986.

[29] Papasouliotis, G. D., and Sotirchos, S. V., 1993. "Heterogeneous kinetics of the chemical vapor deposition of silicon carbide from methyltrichlorosilane". *MRS Online Proc. Libr.,* **334**, p. 111.

[30] Ge, Y., Gordon, M. S., Battaglia, F., and Fox, R. O., 2010. "Theoretical study of the pyrolysis of methyltrichlorosilane in the gas phase. 3. reaction rate constant calculations". *J. Phys. Chem. A.,* **114**(6), pp. 2384–2392.

[31] Dang, K., and Chelliah, H. K., 2022. "Thermal decomposition of methyltrichlorosilane/hydrogen/inert mixtures at conditions relevant for chemical vapor infiltration of sic ceramics". *Int. J. Chem. Kinet.,* **54**(3), pp. 188–202.

[32] Ramanuj, V., Ge, W., Li, M., Sankaran, R., and She, Y., 2023. Modeling the effects of microwave heating on densification in chemical vapor infiltration. Tech. Rep. ORNL/TM-2023/2855, ORNL.

[33] Weller, H. G., Tabor, G., Jasak, H., and Fureby, C., 1998. "A tensorial approach to computational continuum mechanics using object-oriented techniques". *Comput. Phys.,* **12**(6), pp. 620–631.

[34] Lee, G., Law, M., and Lee, V.-C., 2020. "Numerical modelling of liquid heating and boiling phenomena under microwave irradiation using OpenFOAM". *Int. J. Heat Mass Transf.,* **148**, p. 119096.

[35] Sugawara, H., Kashimura, K., Hayashi, M., Ishihara, S., Mitani, T., and Shinohara, N., 2014. "Behavior of microwave-heated silicon carbide particles at frequencies of 2.0–13.5 GHz". *Appl. Phys. Lett.,* **105**(3), p. 034103.

[36] Kern, E., Hamill, D., Deem, H., and Sheets, H., 1969. "Thermal properties of β-silicon carbide from 20 to 2000 C". In *Silicon Carbide–1968*. Elsevier, pp. S25–S32.

[37] Maxwell-Garnett, J. C., 1904. "Xii. colours in metal glasses and in metallic films". *Philos. Trans. R. Soc. Lond. A Math. Phys. Char.,* **203**(359-371), pp. 385–420.

[38] Smith, D. S., Alzina, A., Bourret, J., Nait-Ali, B., Pennec, F., Tessier-Doyen, N., Otsu, K., Matsubara, H., Elser, P., and Gonzenbach, U. T., 2013. "Thermal conductivity of porous materials". *J. Mater. Res.,* **28**(17), pp. 2260–2272.

[39] Ayappa, K., Davis, H., Crapiste, G., Davis, E., and Gordon, J., 1991. "Microwave heating: an evaluation of power formulations". *Chem. Eng. Sci.,* **46**(4), pp. 1005–1016.

[40] Jain, D., Tang, J., Liu, F., Tang, Z., and Pedrow, P. D., 2018. "Computational evaluation of food carrier designs to improve heating uniformity in microwave assisted thermal pasteurization". *Innov. Food Sci. Emerg. Technol.,* **48**, pp. 274–286.

[41] Kalinke, I., Pusl, F., Häderle, F., and Kulozik, U., 2023. "A comparative study of frequency-shifting strategies for uniform and energy-efficient microwave heating in solid-state microwave systems". *Innov. Food Sci. & Emerg. Technol.,* **86**, p. 103388.

[42] D'Ambrosio, R., Aghdam, A. M. G., Cintio, A., Konschak, A., Schmidt, J., Maier, J., Toma, L., Del Campo, L., Rozenbaum, O., Mallah, M., et al., 2024. "Improved densification of SiC_f/SiC composites by microwave-assisted chemical vapor infiltration process based on multifrequency solid-state sources excitation". *J. Eur. Ceram. Soc.*, p. 116950.